Photodissociation Dynamics of 2-Nitropropane and 2-Methyl-2-nitropropane at 248 and 193 nm

Sumana Sengupta, Yogesh Indulkar, Awadhesh Kumar, Suresh Dhanya,* Prakash Dattatray Naik, and Parma Nand Bajaj

Radiation and Photochemistry Division, Bhabha Atomic Research Center, Mumbai 400 085, India

Received: August 5, 2008; Revised Manuscript Received: October 16, 2008

Dynamics of formation of electronically excited NO_2 and formation of OH fragment, during photodissociation of 2-nitropropane (NP) and 2-methyl-2-nitropropane (MNP), were investigated at 193 and 248 nm. The radiative lifetime of the electronically excited NO_2 fragment, observed at 193 nm, was measured to be 1.2 ± 0.1 μs and the rate coefficient of quenching of its emission by MNP was measured as $(2.7 \pm 0.1) \times 10^{-10}$ molecule^{-1} cm^3 s^{-1}. Formation of the ground electronic state of OH was confirmed in both molecules. State selective laser induced fluorescence technique was used to detect the nascent OH ($X\ ^2\Pi$, v″, J″) fragments in different ro-vibrational states, and to obtain information on energy partitioning. Though MNP and NP differ in the types of the available H atoms, the dynamics of OH formation is found to be the same in both. The relative population in different rotational states does not follow Boltzmann equilibrium distribution in both the molecules at 193 and 248 nm. The translational energies of the OH fragments, calculated from the Doppler width, are 21.2 ± 7.2 and 25.0 ± 2.5 kcal mol^{-1} for NP at 248 and 193 nm, respectively. The translational energies of the OH fragments, in the case of MNP, are found to be lower, 17.5 ± 4.1 and 22.0 ± 3.2 kcal mol^{-1}, respectively, at 248 nm 193 nm. These results are compared with the earlier reports on photodissociation of nitromethane (NM), nitroethane (NE), and other nitroalkanes. All possible dissociation pathways of these molecules—NM, NE, NP, and MNP—leading to the formation of the OH fragment were investigated computationally, with geometry optimization at the B3LYP/6-311+G(d,p) level and energy calculation at the MP4(SDQ)/6-311+G (d,p) level. The results suggest that in NM, OH is formed after isomerization to $CH_2N(OH)O$, whereas in all other cases OH is formed from HONO, a primary product of molecular elimination of nitroalkanes, formed with sufficient internal energy.

1. Introduction

Photochemistry and dissociation dynamics of nitro compounds have been extensively investigated[1−5] because of their significant role in explosive chemistry, combustion, atmospheric pollution, etc. It has been shown that even the simplest nitroalkane, nitromethane, undergoes multiple channels of dissociation on photolysis, and therefore its spectroscopy and complex photodissociation dynamics still continue to attract attention.[6−8] The photodissociation of nitromethane (NM) can lead to NO_2, HNO, O atom, and NO fragments,[5−8] which involve the following reactions:

$$CH_3{-}NO_2 + h\nu \rightarrow CH_3 + NO_2 \quad (1)$$

$$\rightarrow CH_2{-}O + HNO \quad (2)$$

$$\rightarrow CH_3{-}ONO \quad (3)$$

$$\rightarrow CH_3{-}NO + O \quad (4)$$

$$\rightarrow CH_3{-}O + NO \quad (5)$$

The studies on product emission spectroscopy and the molecular beam photofragment translational energy spectroscopy have shown that the major photodissociation process on excitation at 193 nm is dissociation of the C−N bond, which can occur through two competing channels, leading to NO_2 fragments in different electronic states.[5] The major part is identified as electronically excited NO_2, whereas the minor part, not clearly characterized,[6] could be another lower excited or ground electronic state of NO_2. In the case of photolysis of higher nitroalkanes, formation of HONO was also observed as a major channel.[1]

$$CH_3CH_2NO_2 + h\nu \rightarrow CH_2CH_2 + HONO \quad (6)$$

Aromatic nitrocompounds also exhibit similar multichannel dissociation on photoexcitation.[9] To understand the competition among the different energetically possible pathways, many theoretical investigations on dissociation dynamics of both aromatic and aliphatic nitrocompounds have been carried out recently.[10,11]

In addition to the above-mentioned photofragments (reactions 1−6), formation of OH was also reported in aromatic[9] and aliphatic[1,3,7] nitrocompounds. Recently, we investigated[12] the OH formation channel on excitation of *o*-nitrotoluene at 193 and 248 nm, and a reaction mechanism was proposed, based on the experiments and calculations.[11] In the case of aliphatic nitroalkanes, formation of the electronic ground state of OH was identified, as a minor channel in the photolysis of NM at 266 nm[7,13] and other nitroalkanes at 282 nm[3] or lower wavelengths,[1,7] using laser induced fluorescence (LIF) technique. The investigations on photodissociation of NM at 266 nm, using time-dependent FTIR emission spectroscopy,[6] did not yield any signal due to OH. This suggests that OH is probably not formed in vibrationally excited state from NM. Zabarnick et al.[13] observed that the electronic ground state of OH ($X^2\Pi_i$), produced by photodissociation of NM at 266 nm, is rotationally much hotter

* Corresponding author.

10.1021/jp806965p CCC: $40.75 © 2008 American Chemical Society
Published on Web 11/17/2008

than that produced from 2-nitropropane (NP).[1] Greenblatt et al.[3] observed that, on excitation at 282 nm, OH was formed only in the case of ethyl or higher nitroalkanes, having a β-hydrogen atom, and not in the case of NM. On the basis of this observation, and the results of isotopic substitution studies, they concluded that on photoexcitation at 282 nm, OH is generated through a transition state involving a five-membered ring, which is not possible in NM. Recently, Yue et al.[7] studied the nascent OH generated from nitroethane (NE) and NM at 266 nm, using the LIF technique. Their results suggest the mechanism of OH formation in NM to be different from that in NE at 266 nm. The above results indicate that formation of OH from nitroalkanes may involve multiple pathways, the pathway in NM being different from those in higher nitroalkanes. The major difference between these molecules is that in NM, only α-hydrogen atom is present, whereas in the higher nitroalkanes, both α- and β-hydrogen atoms are present. Involvement of different types of hydrogen atoms could be responsible for the difference in the mechanism of OH formation. Although OH is a very important intermediate in combustion and atmospheric chemistry, the exact mechanism of OH formation in NM and higher nitroalkanes is not clearly understood. So far, there are no supporting theoretical studies that look into these different mechanisms of OH formation from aliphatic nitrocompounds. In the present study, we have carried out photolysis of 2-nitropropane (NP) and 2-methyl-2-nitropropane (MNP) at 248 and 193 nm, and investigated the dynamics of OH generation. We have also carried out ab initio theoretical calculations, to identify the different channels that lead to formation of OH. These calculations involve optimization of the transition states and calculation of the energetics. NP has both α- and β-hydrogen atoms, whereas MNP has only β- hydrogen atoms. OH fragments were detected by laser-induced fluorescence, and from the recorded LIF excitation spectra, the energy partitioning into the OH fragment was determined. In addition to the OH channel, formation of electronically excited NO_2 also was observed by time-resolved emission spectroscopy, and compared with that from other nitroalkanes.

2. Experimental Section

The details of the laser photolysis−laser induced fluorescence setup used in the present work are described elsewhere.[14] The OH fragments were probed by laser induced fluorescence, using the $A^2\Sigma$ ($v' = 0$)−$X^2\Pi$ ($v'' = 0$) transition, and the vibrationally excited OH radicals, which were also formed, were monitored by $A^2\Sigma$ ($v' = 1$)−$X^2\Pi$ ($v'' = 1$) transition.

The photolysis laser (Lambda Physik Excimer Laser, model Compex-102, Fluorine version) and the probe laser (Quantel dye laser, with frequency doubling module, model TDL90, pumped by a Quantel seeded Nd:YAG laser, model YG980E-20) intersected at the center of the reaction cell. The probe laser-induced fluorescence from this intersection volume was collected with a lens of 50 mm focal length, and detected by a PMT (Hamamatsu, model R928P), which was mounted perpendicular to both the laser beams. The pulse duration of the pump laser beam is 20 ns. A band-pass filter (with λ_{center}= 310 nm, fwhm = 20 nm, $T_{310\ nm} = 10\%$) was used between the collecting lens and the PMT, to cut off scattering from the photolysis laser. In addition, baffles were used in the side arms of the cell, and the optical windows were fixed at the Brewster angle, to minimize scattering. A PC controlled the wavelength scan as well as acquisition of the data, after the signals were integrated by a box-car integrator, SRS 250 and averaged over 30 laser pulses, and digitized. A delay generator controlled the time delay between the photolysis and the probe laser beams. Both the laser beams were unfocused and their intensities were monitored by photodiodes, to correct for the fluctuations. The typical photolysis laser intensity used was in the range of 0.2−0.5 mJ cm^{-2} per pulse at 193 nm. At higher laser intensity, an emission was observed with pump laser alone (discussed in detail in the Results section), and, therefore care was taken to work with very low laser intensity. The linearity of the LIF signal with laser fluence was confirmed for both the photolysis and the probe lasers. The probe laser frequency was calibrated, using an optogalvanic cell (Fe−Ne).

2-Nitropropane (97%) and 2-methylnitropropane (99%) were obtained from Aldrich, and used without further purification, but after 4−5 freeze−pump−thaw cycles. Low pressure (20−40 mTorr) of the sample was maintained in a flow cell, and was measured by a capacitance gauge (Pfeiffer Vacuum, model CMR 263).

The experimental setup for measuring time-resolved UV−vis emission consisted of a Bausch & Lomb monochromator, a PMT (Hamamatsu model R928), and a digital oscilloscope (Tektronics). The sample was allowed to flow in a stainless steel cell, equipped with four perpendicular MgF_2 windows, at a pressure of 20−200 mTorr, and monitored by a capacitance gauge. During the measurement of the emission at wavelengths greater than 350 nm, suitable cutoff filters were used.

3. Computational Details

Ab initio molecular orbital (MO) calculations were performed, using the Gaussian 92[15] program, to investigate the potential energy surface (PES) of the ground state of nitroalkanes. The geometries of the ground electronic states of the nitroalkanes, the various possible products, and the transition state structures were optimized with either HF or B3LYP theory, using 6-311+G(d,p) basis sets. The harmonic vibrational frequencies and the force constants were calculated, to ensure the stationary points on the potential energy surfaces to be true saddle points. All the transition state (TS) structures calculated have only one imaginary frequency and one negative eigenvalue of the force constant matrix. Electronic energies corresponding to the optimized geometries were calculated at the MP2, MP3, and MP4(SDQ) levels, using the same basis sets. With the inclusion of thermal energies, derived from the vibrational frequencies obtained at the B3LYP/6-311+G(d,p) level, the reaction energies and the activation barriers at 298 K were evaluated. For the radical species, the energies were also calculated at the projected MP2 (PMP2) and the projected MP3 (PMP3) levels, to correct for spin contamination, if any. Most of the calculated energies mentioned in this work are at the MP4 (SDQ)/6-311+G (d,p) level.

4. Results

4.1. Emission Studies. Nitroalkanes are known to undergo photodissociation at 193 nm, with cleavage of the C−N bond, leading to formation of electronically excited NO_2 as a primary photoproduct, which gives a prompt emission. We investigated the emission observed on photodissociation of both 2-nitropropane (NP) and 2-methyl-2-nitropropane (MNP) at 193 nm. The emission spectra obtained in both cases are similar, with a maximum around 540 nm, as shown in Figure 1. At higher laser intensities, an emission band at 310 nm was also observed. The variation of signal intensity with photolysis laser intensity was monitored at 540 and 310 nm, and the log−log plot of the fluorescence signal intensity, in the case of MNP, and the pump laser intensity is shown in Figure 1 as an inset. This gives a

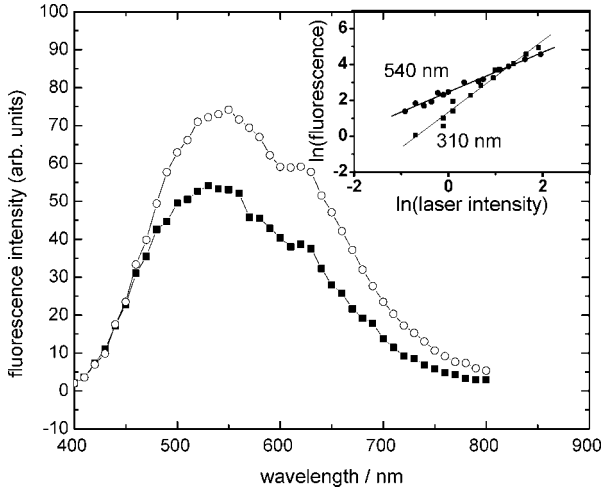

Figure 1. Fluorescence spectra recorded 150 ns after the photolysis of NP (○) and MNP (■) at 193 nm. Inset: Variation of the emission signal from MNP at 540 and 310 nm with intensity of the photolyzing laser (193 nm). Pressure of MNP = 105 mTorr.

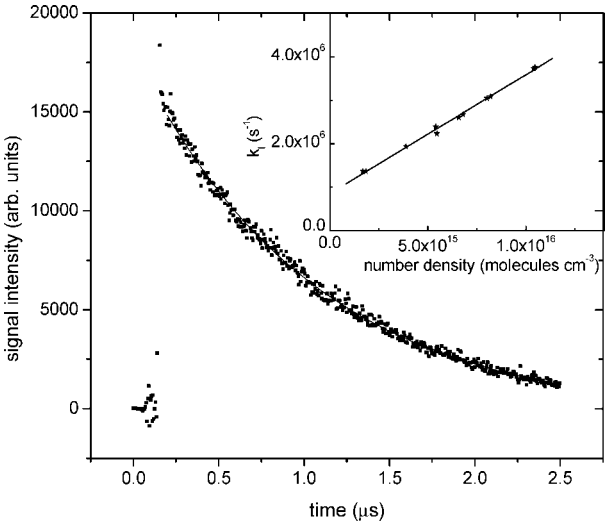

Figure 2. Typical decay trace of emission signal after photolysis at 193 nm, in the case of MNP, at 540 nm. Pressure of MNP = 25 mTorr. Inset: Dependence of the pseudo-first-order decay rate constants of emission on number density of MNP. Slope = $(2.7 \pm 0.1) \times 10^{-10}$ molecule^{-1} cm^3 s^{-1} and intercept = $(8.5 \pm 0.4) \times 10^5$ s^{-1}.

slope of 1.1 ± 0.1 at 540 nm, and 2.0 ± 0.1 at 310 nm, indicating that the origin of the emission at 540 nm is a monophotonic process, and that at 310 nm it is a biphotonic process. The decay kinetics of the emission at 540 nm was also followed as a function of pressure of MNP; a typical temporal profile of the emission at 540 nm and the pseudo-first-order plot of the decay rate coefficient and number density of MNP are shown in Figure 2. The bimolecular rate coefficient for quenching of the excited NO_2 with the parent molecule is calculated from the slope as $(2.7 \pm 0.1) \times 10^{-10}$ molecule^{-1} cm^3 s^{-1}, in the case of MNP. Under similar experimental conditions, excitation at 248 nm did not give measurable emission in this region.

4.2. LIF Studies. The LIF intensities of the nascent OH fragments, formed by the photolysis of NP and MNP at 248 and 193 nm, are found to be directly proportional to the pressure, thereby indicating a unimolecular process. The formation of OH appears to be very fast, within the laser pulse duration of 20 ns. In the case of states with lower J values, after attaining the maximum, the LIF intensity remains invariant, without any

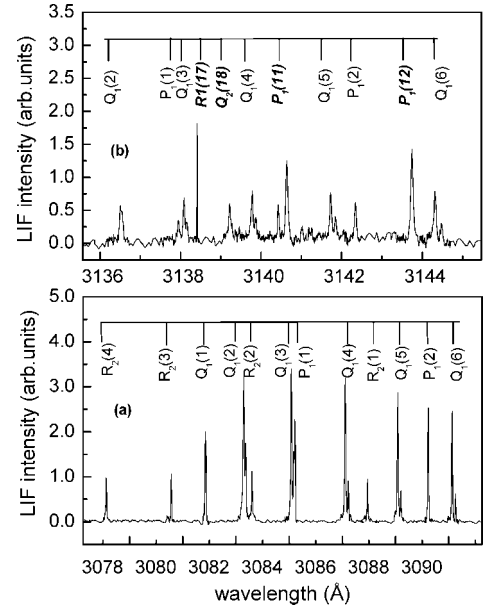

Figure 3. Parts of the LIF excitation spectra of the OH fragment with proper assignments of rotational lines, measured after photolysis of MNP at 193 nm, with a probe laser delay of 50 ns and pump laser intensity of 0.15 mJ cm^{-2}: (a) spectra due to 0−0 transition, pressure of MNP = 20 mTorr; and (b) spectra due to a combination of 0−0 [$R_1(17)$, $P_1(12)$, and $P_1(11)$lines labeled in bold italics] and 1−1 transitions of OH, pressure of MNP = 60 mTorr.

decay up to 4 μs, at both the photolysis wavelengths. The LIF signal intensity of OH and S/N ratio were found to be low on photodissociation of both NP and MNP at 248 nm, probably due to their small absorption cross sections at this wavelength.

4.2.1. LIF Excitation Spectra. Parts of typical LIF spectra of the OH radical produced from MNP at a pump−probe delay of 100 ns, with appropriate assignments,[16] are given in Figure 3. The transitions corresponding to $\Delta N = -1, 0, +1$ are represented by P, Q, and R branches, respectively. Subscripts 1 and 2 represent the transitions from $\Pi_{3/2}$ and $\Pi_{1/2}$ states, respectively. The P and R lines probe the Π^+ (A′) state, whereas Q lines probe the Π^- (A″) state. The individual lines were broadened due to the Doppler effect, but were still well separated to fit the line profile with a Gaussian function. The area under the curve, which is proportional to the population of OH in that particular rotational state, was normalized with respect to the pump and the probe laser intensities and Einstein absorption coefficient, B_{ij},[17] of the transition. It was observed that the population of Π^- (A″) states was less than that of Π^+ (A′) states, in photolysis of both the molecules at 193 and 248 nm, as observed in the case of nitrotoluene.[12] Boltzmann plots of the normalized population distribution of the P-branch in the ground vibrational level of the OH, produced on photolysis at both wavelengths, are shown in Figures 4 and 5 for NP and MNP, respectively. The rotational population distribution is more scattered in the lower energy range, and the plot appears to be curving, indicating that the population of the nascent OH ($v'' = 0$, J'') fragment is not at equilibrium over all the rotational levels J''. During photodissociation of NP and MNP at 193 nm, the vibrationally excited state ($v'' = 1$) of OH was also detected, as shown in Figure 3b.

In addition to the P and the Q line intensities, which provide the Λ-doublet ratio, the initial nonequilibrium is reflected in the spin orbit ratio as well, which is obtained from the measured population of the $\Pi_{3/2}$ state, probed by P_1 and Q_1 lines, to that of the $\Pi_{1/2}$ state, probed by P_2 and Q_2 lines, after multiplying

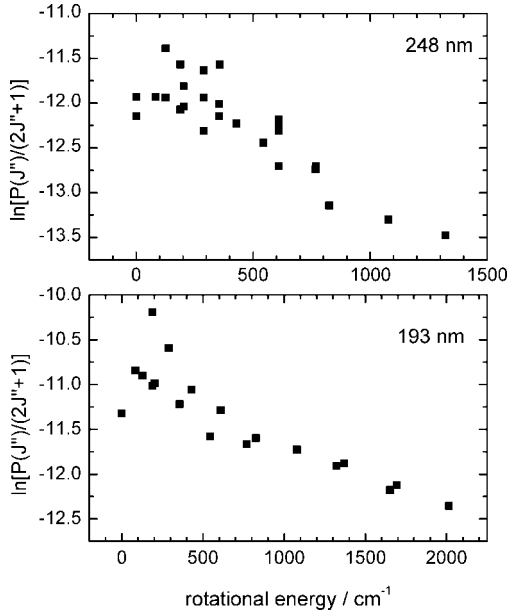

Figure 4. The Boltzmann plot for rotational state distributions of OH ($v'' = 0$), generated from dissociation of 2-nitropropane at 248 (~200 mTorr) and 193 nm (20 mTorr).

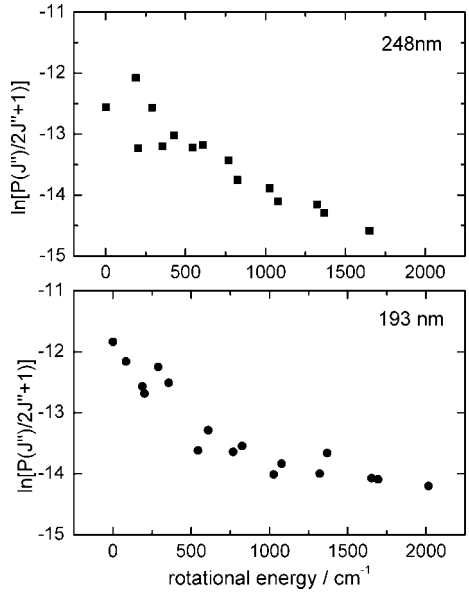

Figure 5. The Boltzmann plot for rotational state distributions of OH ($v'' = 0$), generated from dissociation of 2-methyl-2-nitropropane at 248 (~200 mTorr) and 193 nm (20 mTorr).

by the appropriate statistical weights. The spin orbit population ratios of OH, produced from both NP and MNP on photolysis at 193 nm, are unity, as depicted in Figure 6, except for some deviation at lower rotational levels.

4.2.2. Translational Energy of the Fragments. From the width of the Doppler-broadened rotational lines, the average translational energy of OH can be determined. Doppler profiles were measured for $P_1(2)$, $Q_1(4)$, and $P_1(5)$ lines. A typical profile of the $P_1(2)$ rotational line of OH obtained for NP and MNP, by photolyzing at 248 and 193 nm, is shown in Figure 7. The observed profile is deconvoluted for the instrumental function (probe laser spectral profile), to obtain the corrected Doppler profile, which represents the distribution of the velocity component, v_z, of the OH radicals along the direction of propagation of the probe laser beam. In the present experiments, since the LIF peak profiles are well represented by a Gaussian

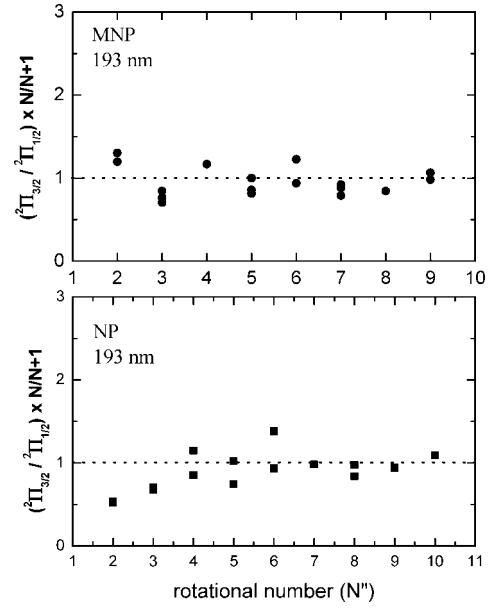

Figure 6. The spin orbit ratio $^2P_{3/2}/^2P_{1/2}$ of OH as a function of rotational quantum number at 193 nm photolysis in the case of NP and MNP.

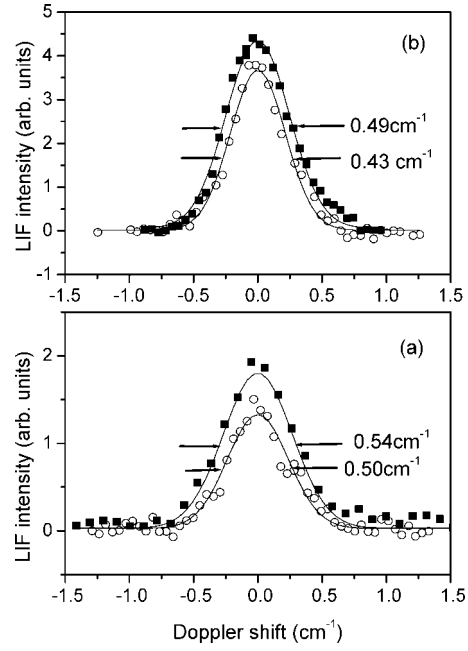

Figure 7. Typical Doppler-broadened rotational lines—$[P_1(2)]$ rotational line of 0−0 band of the A−X system of the OH, fitted by a Gaussian function: (a) 2-nitropropane at 248 (○) and 193 nm (■); and (b) 2-methyl-2-nitropropane at 248 (○) and 193 nm (■).

function, an isotropic velocity distribution can be assumed. The shift in the absorption frequency is given by

$$\upsilon - \upsilon_0 = \nu_z \upsilon_0 / c \tag{7}$$

where υ_0 is the center frequency, υ is the observed frequency, and c is the velocity of light. The corrected Doppler width ($\Delta\upsilon$) is related to the translational temperature T by the following Doppler relationship

$$\Delta\upsilon = \frac{2\upsilon_0}{c}\sqrt{\frac{2kT \ln 2}{m}} \tag{8}$$

where m is the mass of the fragment OH. From the average T_T, average translational energies channeled into OH in the labora-

tory frame are estimated to be 21.2 ± 7.2 and 25.0 ± 2.5 kcal mol^{-1} for photodissociation of NP at 248 and 193 nm, respectively. In the case of MNP, by similar analysis, the average translational energies of the OH fragment in the laboratory frame are estimated to be 17.5 ± 4.1 and 22.0 ± 3.2 kcal mol^{-1}, when photolyzed at 248 and 193 nm, respectively. Due to low signal-to-noise ratio at 248 nm, the error involved in the calculated value for both molecules is higher, as compared to that at 193 nm.

5. Discussion

5.1. Emission. Nitroalkanes have two broad absorption bands, a weak band centered at around 280 nm, and a stronger band centered at around 200 nm. The band at the longer wavelength was assigned to $\pi^* \leftarrow$ n transition, and the strong band at 200 nm to $\pi^* \leftarrow \pi$ transition, both located at NO_2.[18] More recently, on the basis of theoretical calculations, the long wavelength band has been assigned to the $\pi^*(NO) \leftarrow \sigma$ (CN) transition.[19] All the experimental studies on nitroalkanes show that the dissociation of the C−N bond is the primary photolysis channel at 193 nm, which occurs in the picosecond time scale, giving electronically excited NO_2 as a major product.[5,20] But on photodissociation at 266 nm, the major channel is the formation of the ground state of NO_2.[2] The dynamics of C−N dissociation has been studied in the case of NM, both experimentally and theoretically. Using emission spectroscopy and molecular beam photofragment translational energy spectroscopy, Butler et al.[5] identified two photodissociation channels in NM at 193 nm. The major channel leads to fast methyl radicals and NO_2 in an emitting electronically excited state, which is identified as the 1^2B_2 state, and the minor channel leads to slower methyl radicals. On the basis of the polarized emission spectroscopy of NM at 200 and 218 nm, and considering orbital symmetries electronic states of NM and NO_2, Lao et al.[20] assigned the major channel to electronic predissociation of the 1^1B_2 state of NM to CH_3 and NO_2 (1^2B_2) and the minor channel to vibrational predissociation on the 1^1B_2 surface, leading to $CH_3 + NO_2$ (2^2B_2). Arenas et al.[19,21] studied the ground and the excited state potential energy surfaces of NM, and correlated with the photodissociation at 193 nm. The earlier calculation[19] showed that the initial excitation of NM to the 2A″ state is followed mainly by internal conversion to the 2A″ state, which dissociates to form the $^2B_1$ state of NO_2, as a major channel, and partly by direct dissociation to form NO_2 ($^2A_2$) as a minor channel. However, their recent calculations[21] suggest fast radiationless decay through conical intersections, deactivating the initially formed S_3 (A″) excited state, leading to NO_2 ($^2B_2$) formation from the lower excited state of NM, and NO_2 ($^2A_1$) formation from the ground state. Thus, both experimental and theoretical studies agree on the formation of the NO_2 ($^2B_2$) state as the major channel, though the minor product is not assigned unambiguously.

The emission spectra obtained in the present study, after photoexcitation of NP and MNP at 193 nm, are similar to the spectra obtained by Butler et al. for NM, NE, and NP, with the maximum at around 540 nm. Similar emission characteristics of all these nitroalkanes, including MNP, which is reported here, indicate that there is not much intramolecular transfer of energy from the excited NO_2 group to the alkyl group during the C−N bond dissociation. This result supports the mechanism of very fast radiationless decay through conical intersections, and fast dissociation of the C−N bond, before randomization of the excitation energy. A similar conclusion was drawn from the earlier emission studies on dissociation at 193 nm[5] as well as LIF studies[2] on NO_2 fragments formed by photolysis at 266 nm.

We measured the emission lifetime at 540 nm to be 1.1 μs, at a pressure of 25 mTorr, and 0.5 μs at a pressure of 105 mTorr of MNP. Butler et al.[5,21] reported an emission lifetime of 35 ± 5 μs, which agrees well with the reported lifetime[22] for emission from the $^2B_2$ state of NO_2. The lifetimes measured in the present studies are much shorter as compared to that observed for the excited NO_2. NO_2 is known to have an anomalous long radiative lifetime as well as sharp variations of lifetime in certain wavelength regions[23] due to vibronic interactions of the excited states $^1A_2$ and $^2B_2$, which are known to cross along a C_{2v} path,[24] and the ground state. From the detailed study of NO_2 fluorescence, it was concluded that no NO_2 excited state could have a lifetime of the order of 1 μs.[25] However, a lifetime of the order of 1 μs has been reported in some studies.[2,26] During the picosecond LIF study of the ground state NO_2, formed by the collisionless photodissociation of NM at 264−238 nm, Goldberg et al.[26] reported a lifetime of 1.6 μs at a pressure of 100 mTorr of NM. In a similar experiment, Mialocq and Stephenson[2] measured the fluorescence lifetimes of NO_2, formed by the collisionless photodissociation of nitroalkanes at 266 nm, monitored by LIF at 527 nm excitation. In the case of NM, the LIF at 532 nm was found to decay monoexponentially, in the pressure range of 0.1−2.5 Torr, with a lifetime of 2.15 μs at 120 mTorr of pressure. In the present study, we observed an emission lifetime of 0.5 μs, on photolysis of 105 mTorr of pressure of MNP at 193 nm. The lower lifetime, in the case of MNP, as compared to that in the case of NM, is not unusual, because Mialocq and Stephenson[2] have already observed such a reduction in emission lifetime with higher nitroalkanes. They have reported that the lifetime of emission changes from 0.44 μs at 1 Torr, in the case of NM, to 0.32 μs at 1 Torr of pressure, in the case of 1-nitropropane, due to more efficient collisional energy transfer in the case of bigger molecules. The least-squares fit of the variation of the decay rate constant of emission, with pressure of MNP (Figure 2), yields an intercept of (8.5 ± 0.4) × 10^5 s^{-1}, corresponding to a lifetime of 1.2 ± 0.1 μs and a quenching rate constant of (2.7 ± 0.1) × 10^{-10} $molecule^{-1}$ cm^3 s^{-1}. The corresponding intercept value observed by Mialocq and Stephenson[2] for NO_2 emission (LIF) from NM is 5.8 μs, higher than the 1.2 μs value observed by us. The quenching rate coefficient is 6.4 × 10^{-11} $molecule^{-1}$ cm^3 s^{-1}, which is smaller than that determined in the present study, as expected for a smaller nitroalkane. However, all these observations (refs 2 and 26 and the present work) are very different from the reported fluorescence lifetime of NO_2, probably indicating complex secondary processes occurring in the system, or the presence of more than one emitting species.

Another possibility for the very short emission lifetime observed here is the contribution of emission from the higher excited states of NO_2 formed by a sequential two-photon absorption. Butler et al.[5] have noted that the lower excited state of NO_2 has a very high absorption cross section at 193 nm, and after absorbing an additional 193 nm photon, the molecule dissociates to NO and O atom. Since dissociation of the C−N bond is very fast (in ps), NO_2 formed can absorb more photons from the same laser pulse (20 ns). In recent experiments, where NO_2 was photolyzed by a 193 nm laser, the emission spectra and lifetimes showed a cascading nature, indicating emission from different states.[27] They observed an emission maximum at 480 nm, at 150 ns after the laser pulse, which shifted to a higher wavelength (520 nm) at 1 μs. The radiative decay in

this work was biexponential, with 0.2 and 0.6 μs lifetimes. Recently, during the lifetime measurements of NO_2 fluorescence[28] in the wavelength range of 423−462 nm, in addition to the constant component of 35−48 μs, short lifetime components of 1−6 μs started appearing above 5 mTorr of NO_2 pressure, and components of lifetime of the order of 0.1 μs were also observed at pressures above 10 mTorr. The origin of these short components is not completely understood. With this complex behavior of the emission lifetime of NO_2, it is difficult to explain the short lifetime observed in the present work unambiguously.

5.2. Formation of OH. In the present experiments on photodissociation of NP and MNP at 248 and 193 nm, the energy distribution pattern in the OH product has been found to be very similar. The translational energy of the OH fragment is in the same range, for both molecules, with slightly higher energy (3 kcal mol^{-1}) in the case of NP at both wavelengths. Also, the translational energy of OH produced on photodissociation at 193 nm (photon energy = 148.3 kcal mol^{-1}) is more than that at 248 nm (photon energy is 115.4 kcal mol^{-1}), for both molecules. This difference is only 4−5 kcal mol^{-1}, though the difference in the photon energies is 35 kcal mol^{-1}. This could be due to the fact that OH is not formed by a direct dissociation step from one of the excited states of the molecule, and the mechanism of photodissociation involves stable or unstable intermediates.

The present results of photodissociation of NP and MNP at 248 and 193 nm show that the nascent OH fragments do not have an equilibrium distribution in the rotational levels, as indicated by the curving Boltzmann's plots (Figures 5 and 6). Very similar results were obtained by Greenblatt et al. during photodissociation of NE and higher nitroalkanes at 282 nm[3], and recently that of NE at 266 nm.[7] However, in the case of OH generation by one-photon UV photolysis (222, 248, and 308 nm) of NP[1] under collision-free conditions, the populations of the lower rotational states (within 800 cm^{-1} rotational energy) show a linear Boltzmann distribution, with a temperature of about 370 K. If we analyze carefully (Figure 4), the initial points of lower energies up to 800 cm^{-1}, in the present study also, lie on a straight line, with a lower rotational temperature (600 K), and the later points at higher energies show a higher rotational temperature (2700 K). Thus, the lower rotational temperature (600 K) observed in the present study is not very different from that given in the previous report.[1] The curving of the Boltzmann plot can be due to either formation of two types of OH fragments from two different mechanisms, each with a rotational equilibrium corresponding to a rotational temperature, or to formation of OH fragments by a single mechanism with nonequilibrium distribution in the rotational states (discussed vide infra). In contrast, the populations of the OH fragment from photodissociation of NM at 266 nm were found to follow good Boltzmann distribution, characterized by a rotational temperature of 2045 ± 150 K for the $X^2\Pi_{3/2}$ state, and 1920 ± 150 K for the $X^2\Pi_{1/2}$ state, respectively.[7] These rotational temperatures are closer to that observed for the higher rotational energy states of OH in the present studies of NP and MNP. Interestingly, the previous studies on photodissociation of nitroalkanes at 282 nm failed to detect OH formation in the case of NM, whereas it was detected in all other higher nitroalkanes, with a similar non-Boltzmann nascent distribution of the OH rotational population. Thus, it appears that the mechanism of formation of OH for NM is different from that in the higher nitroalkanes.

5.3. Transition State Calculations. Several groups have studied photodissociation of NM at different wavelengths experimentally, and the results are not consistent, especially with respect to formation of the OH fragment, as mentioned in the Introduction. The mechanism of formation of OH is not well established, and the difference between dissociation dynamics of NM and that of the other nitroalkanes is also not well understood. Theoretical calculations have been carried out on the ground electronic state, to understand the different channels of thermal dissociation as well as photodissociation of nitroalkanes,[19,21] but there are no theoretical studies to understand the OH generating channel(s). As discussed in the previous section, the excited state calculations on NM have predicted fast radiationless decay, through conical intersections, from the initially populated excited state to the lower/ground electronic states of NM, before dissociation. The dissociation of the C−N bond leads to formation of electronically excited NO_2 as the major channel and formation of the ground/lower electronic state of NO_2 as a minor channel, within less than 6 ps. Thus, it can be assumed that all other competing dissociation and rearrangement channels occur from the ground electronic state. Therefore, we have carried out ab initio calculations on different channels only from the ground electronic state of nitroalkanes.

In the present study, we have considered different possibilities of OH formation from NM, NE, NP, and MNP, along with the major channel of C−N bond dissociation, and compared their energetics. The results are discussed here.

In the case of NM, the different possible channels, reactions 1−5, are already given in the Introduction. Zabarnick et al.[13] reported formation of OH as an additional channel, and the mechanism of formation was considered to probably involve isomerization to an aci-nitromethane form. This aciform was proposed in solution, though its stability has not been demonstrated in the gas phase. Similar isomerization reactions involving migration of a H atom from carbon to oxygen, the cis and the trans forms of the product, as well as the resonance structures, were considered by Hu et al.,[29] during their theoretical study on unimolecular dissociation pathways of NM.

$$CH_3NO_2 \rightarrow CH_2 = N^+(OH)O^- \qquad (9)$$

Though this structure is not confirmed in the gas phase, this rearranged form, $CH_2N(O)OH$, is termed as aciform for convenience. N−O bond dissociation from this structure (reaction 10) can lead to formation of OH.

$$CH_2N(O)OH \rightarrow OH + CH_2NO \qquad (10)$$

Hu et al.[29] studied the potential energy surfaces for unimolecular isomerization and dissociation of NM, at the G2MP2/B3LYP/6-311++G(2d,2p) level of theory. The calculations showed that the C−N bond dissociation, reaction 1, is the lowest energy channel (61.9 kcal mol^{-1}), with a barrier lower than those of isomerization reactions to methyl nitrite and aci-nitromethane, reactions 3 and 10, by 2.7 and 2.1 kcal mol^{-1}, respectively. Although unimolecular dissociation pathways from these isomerized products were investigated, bond dissociation energy of the N−O bond in aci-nitromethane was not computed. Our present calculations at the MP4(SDQ) level show that the energy required for the C−N bond dissociation in NM, leading to NO_2, is 56.2 kcal mol^{-1}, which is lower than that calculated at the G2MP2 level earlier, but better than the B3LYP value. The barrier for rearrangement to aciform is calculated as 66.4 kcal mol^{-1}, and the N−OH bond dissociation energy in the rearranged molecule is 63.2 kcal mol^{-1}. Values of all these energies are given in Table 1. The most stable aciform is cis, where NO and OH are oriented in the same direction with respect to the N−O bond, lying at about 23.4 kcal mol^{-1} above the parent molecule. A four-membered ring transition state, with a dihedral

TABLE 1: Bond Dissociation Energies and Energy Barriers (in kcal mol^{-1}) for Different Reactions from Excited Nitroalkanes: Nitromethane, Nitroethane, 2-Nitropropane, and 2-Methyl-2-nitropropane

channel	nitromethane	nitroethane	2-nitropropane	2-methyl-2-nitropropane
simple bond rupture: $RNO_2 \rightarrow R + NO_2$	55.0 (53.8)[a]	56.8 (53.5)[a]	58.9 (52.4)[a]	54.5 (49.3)[a]
	61.9[b]	53.8[e]	52.6[e]	
	60.1,[c] 58.5[d]	57.7,[c] 56.4[f]	53.4[f]	
HONO elimination		50.2 (41.9)[a]	49.7 (38.9)[a]	46.5 (38.1)[a]
		42.1[e]	39.2[e]	
		45,[c] 45.0[f]	40[c]	
isomerization to aciform: $RNO_2 \rightarrow R'NOH$	66.4 (61.6)[a] 64[b]	66.2 (60.5)[a] 64.5[e]	69.6 (63.6) [a]63.2[e]	
$R'NOH \rightarrow R'N + OH$	38.0 (34.1)[a]	46.0 (41.6)[a]	40.6 (36.5) [a]	
isomerization to nitrite	64.6[b]	59.8[e]	55.6[e]	62.4 (54.4)[a]

[a] Present calculation with geometries optimized at the B3LYP/6-311+G(d,p) level and energies calculated at the MP4(SDQ) level and that calculated at the B3LYP level (in parantheses) with the same basis sets. [b] G2MP2 calculation from ref 29. [c] Experimental value from ref 30. [d] Experimental value from ref 34. [e] DFT calculation from ref 10 [f] Estimated value from ref 35.

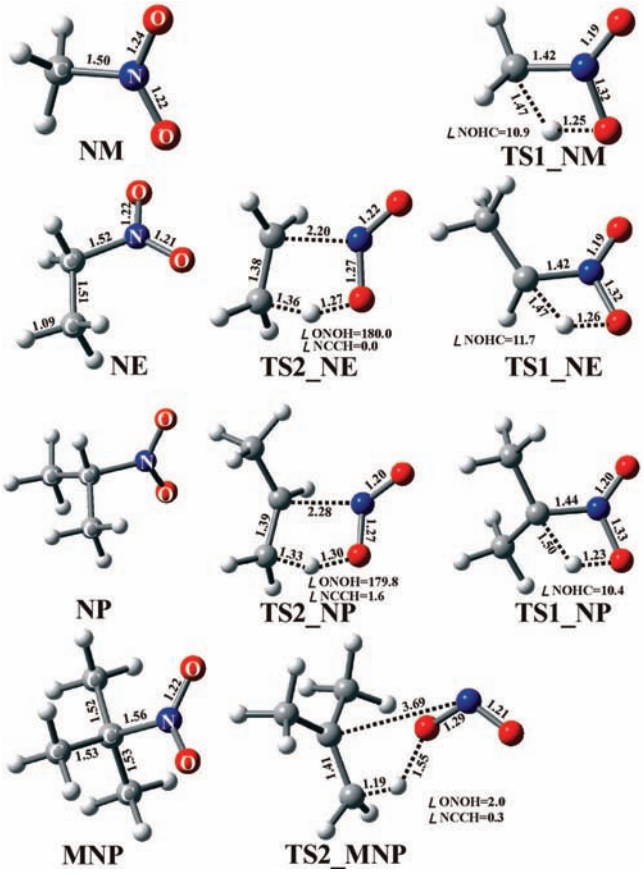

Figure 8. Optimized structures of nitroalkanes, each along with TS, are shown in a row: NM (nitromethane), NE (nitroethane), NP (2-nitropropane), and MNP (2-methylnitropropane). Transition states for HONO elimination (TS1) and rearrangement to aciform (TS2) for these nitroalkanes. Structures are optimized at the B3LYP/6-311+G(d,p) level of theory. Bond distances marked are in angstroms and dihedral angles in degrees.

angle ∠NOHC of 10.9°, is identified for this rearrangement, as shown in Figure 8, TS1_NM. The C−H bond is stretched to 1.47 Å, bringing the H atom closer to the O atom, with the O−H distance of 1.25 Å. One N−O bond, in which the H atom is becoming attached to the O atom, is elongated to 1.32 Å, and the other one is 1.19 Å. The other possibility is rearrangement of $CH_2N(O)OH$ to $CH_2(OH)NO$, as considered by Hu et al.[29] Although $CH_2(OH)NO$ is more stable than even NM, the barrier involved was found to be much higher, 76 kcal mol^{-1}. So this channel was not considered in the present calculations.

For higher nitroalkanes, the number of energetically possible dissociation pathways is more. Table 1 lists the bond dissociation energies and the activation barriers calculated for different channels in nitroalkanes in the present study, along with some earlier reported (calculated or experimental) values. It can be seen that in all the nitroalkanes, with more than one C atom, concerted molecular elimination of HONO, reaction 11, is the lowest energy channel,[10] competing with the C−N bond breaking, reaction(12, due to the availability of an H atom at the β position.

$$CH_3CH(CH_3)NO_2 + h\nu \rightarrow CH_2CH(CH_3) + HONO \quad (11)$$

$$\rightarrow CH_3CH(CH_3) + NO_2\ (1^2B_2) \quad (12)$$

From Table 1, it can be seen that the B3LYP energy calculated for the C−N bond dissociation in nitroalkanes decreases with substitution, due to the increased stability of the free radical formed. Similarly, the barriers for HONO elimination and rearrangement to nitrite decrease with substitution. If the HONO formed in reaction 11 has sufficient excess energy, it can dissociate, giving OH and NO.

$$HONO \rightarrow OH + NO \quad (13)$$

Enthalpy change of 48 kcal mol^{-1} is reported for reaction 13.[30] The present calculations give values of 45.2 and 48.2 kcal mol^{-1} at B3LYP and MP2 levels, respectively. In all our present calculations, MP4(SDQ) values are considered (Table 1) for comparison, which are closer to the available experimental values, except in the case of HONO, because the MP2 value is found to be closer to the experimental value.

The nitroalkane molecule can also isomerize to nitrite, reaction 14, and aciform, reaction 15.

$$CH_3CH(CH_3)NO_2 + h\nu \rightarrow CH_3CH(CH_3)ONO \quad (14)$$

$$\rightarrow CH_3C(CH_2)N(O)OH \quad (15)$$

The transition state for formation of aciform, in the case of higher nitroalkanes, is similar to that for nitromethane, as discussed earlier. The four-membered ring transition states in NE, TS1_NE and in NP, TS1_NP are also found to be almost planar, with a dihedral angle of ~10°. Subsequent dissociation of the N−OH bond of aciform (reaction 16) can also give rise to OH.

$$CH_3C(CH_2)N(O)OH \rightarrow CH_3C(CH_2)NO + OH \quad (16)$$

In the case of elimination of HONO, the transition states for NE, NP, and MNP (TS2_NE, TS2_NP, and TS2_MNP in Figure 8) are five-membered rings of C, C, N, O, and H, with all of them in the same plane, ∠CCH and ∠CCN very near to 90°, and ∠NCCH very near to zero. The H atom from the β-carbon atom is transferred to the O atom. The C−H and the C−N bonds

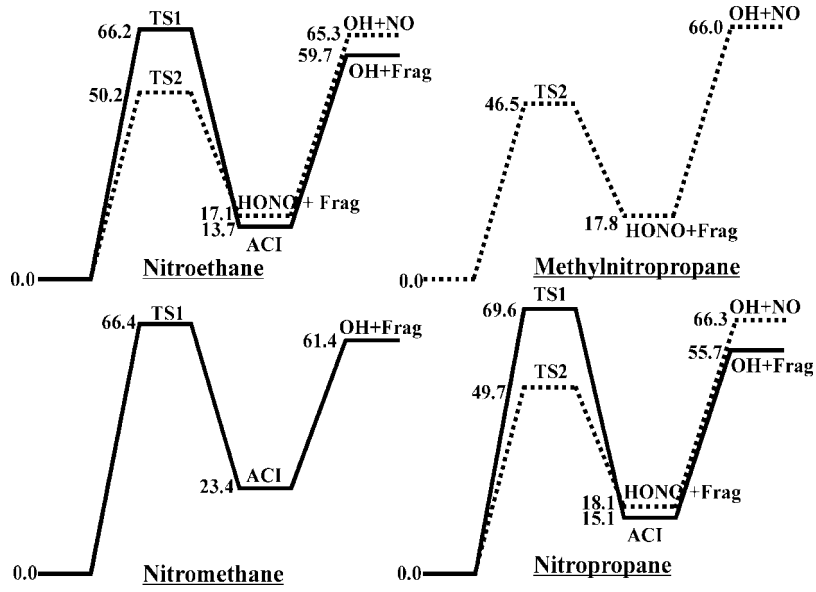

Figure 9. Schematic energy diagram of OH generating channels from nitroalkanes, nitromethane (NM), nitroethane (NE), 2-nitropropane (NP), and 2-methyl-2-nitropropane (MNP): solid line via HONO and dotted line via aciform, TS1 transition state for HONO elimination and TS2 transition state for rearrangement to aciform. Energies (in kcal mol^{-1}) are calculated at MP4(SDQ)/6-311+G(d,p) level, after optimizing geometries at the B3LYP/6-311+G(d,p) level of theory.

are already elongated in the TS to 1.36 and 2.2 Å, respectively, in the case of NE. The dihedral angle of the HONO moiety in the TS is 180° in NE, indicating formation of the trans isomer of HONO. The bond angle ∠HON is 94°. The TS structure for HONO elimination from NP remains similar to that from NE. However, in the case of MNP (Figure 8), the C−N bond is extensively elongated to 3.69 Å, and ∠HON is also higher, i.e.,150°. Here, the second O atom is cis to the hydrogen being transferred, leading to formation of the cis isomer of HONO. This different TS structure in MNP could be due to the steric hindrance from the methyl groups. In the case of all these molecules, the C−C bond, in the TS for HONO elimination, has a partial double bond character, indicated by a decrease of its bond length to ∼1.4 Å.

Another possibility of HONO elimination, involving an α-hydrogen atom, also can be considered in the case of NM, NE, and NP, leading to the formation of a carbene, and OH can be formed by dissociation of HONO. In the case of NM, our attempts to identify the transition state for this reaction, where the α-H atom migrates to O of NO_2, with simultaneous breaking of the C−N bond, lead to the TS corresponding to the aciform only. The maximum stability of the carbene is expected to be in the case of NP, but a transition state could not be optimized even for this molecule. The endothermicity of the reaction, which leads to a carbene and HONO,

$$CH_3CH(CH_3)NO_2 + h\nu \rightarrow (CH_3)_2C: + HONO \quad (17)$$

was calculated to be 83.7 kcal mol^{-1} at the MP4(SDQ) level. Using tabulated heat of formation values,[30] Butler et al.[5] calculated endothermicity (ΔH^0_{300}) of a similar reaction in the case of NM to be 85.6 kcal mol^{-1}, which is comparable with the present value. It is evident that HONO, produced by this reaction from NP, cannot lead to the formation of OH with a translational energy of 25 kcal mol^{-1} even at 193 nm. Similarly, formation of OH in the case of photodissociation of NM at 266 nm (108 kcal mol^{-1}) also cannot be explained by this mechanism, because it is not energetically feasible. In addition to these pathways, Hu et al.[29] have considered similar formation of carbene and elimination of HONO from the rearranged molecule, $CH_2N(O)OH$, in the case of NM. The enthalpy of this reaction was calculated to be 84.6 kcal mol^{-1}, higher than the N−OH bond dissociation energy. This pathway also can be neglected based on the same facts given above. In higher nitroalkanes, formation of HONO after rearrangement to nitrite form[10] is possible and it is energetically compatible with the experimental observations. However, this is not considered here, because the energy barrier for nitrite formation is higher than that for direct HONO elimination (Table 1). Another possibility of formation of OH is its direct elimination along with NO—a 3-body reaction, which was also tried, but no TS could be optimized corresponding to this channel. So, we conclude that OH is formed either through aciform or through the HONO formed, with the involvement of a β-carbon atom, as a secondary dissociation product.

From the potential energy scheme given in Figure 9, it can be seen that for all the nitroalkanes investigated, their rearrangement to aciform, and subsequent dissociation, as well as elimination of HONO, followed by its dissociation, are energetically feasible with a photon of 282 nm (101.5 kcal mol^{-1}), or lower wavelength. Thus, based on the available photon energy, it is not possible to distinguish these two pathways of OH formation. However, the HONO elimination channel is not feasible, in the case of NM, and OH has to come from the aciform only. In NE and NP, OH can come from either aciform or HONO, whereas the probability of formation of the aciform is negligible in MNP, and OH has to be formed through HONO. In our experimental conditions, we have observed a very similar energy distribution pattern of the nascent OH product in the photodissociation of NP and MNP, suggesting that the OH formation pathways are similar in these molecules. The common mechanism of OH formation in NP and MNP is that involving formation of HONO. Thus, it may be concluded that OH is formed via aciform in NM, whereas in the higher nitroalkanes, it is formed via mainly HONO elimination, involving the β-carbon atom, with probably some varied minor contributions from the aciform mechanism. This explains the different behavior of OH formation dynamics in the case of NM. The presence of primarily a common precursor in all these higher

nitroalkanes may be the reason for similar translational energies in NP and MNP—the translational energy of OH in the case of NP being higher by only by 3−4 kcal mol^{-1} than that in the case of MNP. The internal energy of HONO formed is expected to be higher in the case of NP, due to the smaller counter fragment, as compared to that in MNP. This could be the reason for the marginally higher translational energy of OH formed in the case of NP. This fact can be easily seen assuming a pure statistical model for dissociation. For this assumed case, we calculated the internal energy of the products of reaction 11 for both NP and MNP, and found that internal energy partitioned to HONO in NP is 15% higher than that in MNP for both photon energies.

We calculated unimolecular rates for the two channels, rearrangement to aciform, and elimination of HONO, on excitation of NP at 193 nm, using the Rice-Ramsperger-Kassel-Marcus (RRKM) statistical theory.[31,32] The rotational constants, vibrational frequencies of both parent molecule and transition states, and the barrier energies for both channels were used for calculating RRKM rates. The results show that the rates of HONO elimination and rearrangement to aciform are 5.4×10^9 and 1.7×10^7 s^{-1}, respectively, at room temperature. Hence, in molecules like NE and NP, where HONO elimination as well as rearrangement to the aciform are possible, the HONO elimination channel will predominate, because its rate is approximately 300 times faster than that of rearrangement to aciform. This also supports our earlier conclusion based on the observed dynamics that, in NE, NP, and MNP, OH generation is via mainly the HONO channel. This calculation is done only to compare the rates of these two channels under identical energy distribution among different modes of the parent molecule. A pure statistical model is not valid in the present case, as indicated by the high translational energies of OH fragments.

Very recently, the NO radical formation was observed during photolysis of NE[33] at 266 nm, using the LIF technique. The rotational state distribution was fitted to a straight line, but the plot appeared to be curving, as in the case of formation of OH from photodissociation of NP and MNP. NO can be formed by dissociation of the nitrite form, or from dissociation of NO_2 and HONO. The similarity with the OH rotational distribution pattern may be indicating a common origin, at least for a part of the NO and the OH produced.

6. Conclusion

The emission from NO_2 fragment and the dynamics of formation of OH fragment, during photodissociation of 2-nitropropane and 2-methyl-2-nitropropane, have been investigated. The experimental results are compared with the previous reports on nitromethane and other higher nitroalkanes. From the variation of the emission lifetime of NO_2 with pressure of 2-methyl-2-nitropropane, the radiative lifetime and the rate constant of emission quenching by 2-methyl-2-nitropropane have been determined as 1.2 μs and 2.7×10^{-10} $molecule^{-1}$ cm^3 s^{-1}, respectively.

The formation of OH fragment was confirmed during the photodissociation of 2-nitropropane and 2-methyl-2-nitropropane at 248 and 193 nm, which was monitored, using the state selective LIF technique. The translational energies of the OH fragment were measured to be 21.2 ± 7.2 and 25.0 ± 2.5 kcal mol^{-1} for photodissociation of 2-nitropropane at 248 and 193 nm, respectively. The translational energies in the case of OH from 2-methyl-2-nitropropane were found to be lower, 17.5 ± 4.1 and 22.0 ± 3.2 kcal mol^{-1}, when photolyzed at 248 and 193 nm, respectively. In all these cases, a nonequilibrium distribution of the rotational population was observed, indicated by curving of the Boltzmann plots. Similar behavior was observed in the case of nitroethane and nitropropane, whereas a perfect Boltzmann distribution, with a high rotational temperature (2000 K), distinctly different from other nitroalkanes, was reported in the case of nitromethane. Ab initio calculations were carried out to understand and compare the various possible pathways of formation of OH in NM, nitroethane, 2-nitropropane, and 2-methyl-2-nitroproane. Our theoretical calculations, combined with the experimental results, suggest that in nitroethane and higher nitroalkanes, OH is formed from dissociation of HONO, the product of concerted molecular elimination, whereas in nitromethane, it is formed from rearranged structure of the parent molecule, $CH_2N(O)OH$.

Acknowledgment. The authors are grateful to Dr. S. K. Sarkar and Dr. T. Mukherjee for their constant encouragement and support during the course of this work.

References and Notes

(1) Radhakrishnan, G.; Parr, T.; Wittig, C. *Chem. Phys. Lett.* **1984**, *111*, 25.
(2) Mialocq, J. C.; Stephenson, J. C. *Chem. Phys.* **1986**, *106*, 281.
(3) Greenblatt, G. D.; Zuckerman, H.; Haas, Y. *Chem. Phys. Lett.* **1986**, *134*, 593.
(4) Kwok, W. M.; Hung, M. S.; Phillips, D. L. *Mol. Phys.* **1996**, *88*, 517.
(5) Butler, L. J.; Krajnovich, D.; Lee, Y. T.; Ondrey, G.; Bersohn, R. *J. Chem. Phys.* **1983**, *79*, 1708.
(6) Wade, E. A.; Reak, K. E.; Li, S. L.; Clegg, S. M.; Zou, P.; Osborn, D. L. *J. Phys. Chem. A* **2006**, *110*, 4405.
(7) Yue, X.; Sun, J.; Wei, Q.; Yin, H.; Han, K. *Chin. J. Chem. Phys* **2007**, *20*, 401.
(8) Park, M. S.; Jung, K.-H.; Upadhyaya, H. P.; Volpp, H.-R. *Chem. Phys.* **2001**, *270*, 133.
(9) Lin, M. F.; Lee, Y. T.; Ni, C.-K.; Xu, S.; Lin, M. C. *J. Chem. Phys.* **2007**, *126*, 64310.
(10) Denis, P. A.; Ventura, O. N.; Le, H. T.; Nguyen, M. T. *Phys. Chem. Chem. Phys.* **2003**, *5*, 1730.
(11) Chen, S. C.; Xu, S. C.; Diau, E.; Lin, M. C. *J. Phys. Chem. A* **2006**, *110*, 10130.
(12) Sengupta, S.; Upadhyaya, H. P.; Kumar, A.; Dhanya, S.; Naik, P. D.; Bajaj, P. N. *Chem. Phys. Lett.* **2008**, *452*, 239.
(13) Zabernick, S.; Fleming, J. W.; Baronavski, A. P. *J. Chem. Phys.* **1986**, *85*, 3395.
(14) Upadhyaya, H. P.; Kumar, A.; Naik, P. D.; Sapre, A. V.; Mittal, J. P. *Chem. Phys. Lett.* **2001**, *349*, 279.
(15) Frisch, M. J. et al. *Gaussian 92*, Revision E.1; Gaussian, Inc.: Pittsburgh, PA, 1992.
(16) Dieke, G. H.; Crosswhite, H. M. *J. Quant. Spectrosc. Radiat. Transfer* **1961**, *97*, 2.
(17) Chidsey, I. L.; Crosley, D. R. *J. Quant. Spectrosc. Radiat. Transfer* **1980**, 187.
(18) Mijoule, C.; Odiot, S.; Fliszar, S.; Schnur, J. M. *THEOCHEM* **1987**, *149*, 311.
(19) Arenas, J. F.; Otero, J. C.; Pelaez, D.; Soto, J. *J. Chem. Phys.* **2003**, *129*, 7814.
(20) Lao, K. Q.; Jensen, E.; Kash, P. W.; Butler, L. J. *J. Chem. Phys.* **1990**, *93*, 3958.
(21) Arenas, J. F.; Otero, J. C.; Pelaez, D.; Soto, J. *J. Chem. Phys.* **2005**, *122*, 84324.
(22) Stevens, C. G.; Swagel, M. W.; Wallace, R.; Zare, R. N. *Chem. Phys. Lett.* **1973**, *18*, 456.
(23) Santoro, F.; Petrongolo, C. *J. Chem. Phys.* **1999**, *111*, 9651.
(24) Davidson, E. R.; Borden, W. T. *J. Phys. Chem.* **1983**, *87*, 4783.
(25) Keyser, L. F.; Levine, S. Z.; Kaufman, F. J. *Chem. Phys.* **1971**, *54*, 355.
(26) Schoen, P. E.; Marrone, M. J.; Schnur, J. M.; Goldberg, L. S. *Chem. Phys. Lett.* **1982**, *90*, 27224.
(27) Upadhyaya, H. P.; Kumar, A.; Naik, P. D.; Mittal, J. P.; Volpp, H.-R. To be submitted for publication.
(28) Sivakumaran, V.; Subramanian, K. P.; Kumar V. *J. Quant. Spectrosc. Radiat. Transfer*, **2001**, *69*, 513.
(29) Hu, W.-F.; He, T.-J.; Chen, D.-M.; Liu, F.-C. *J. Phys. Chem. A* **2002**, *106*, 7294.

(30) Benson, S. W.; O'Neal, H. E. *Kinetic data on gas phase unimolecular reactions*; National Bureau of Standards: Washington, D.C., 1970; Library of Congress Card Catalogue No. 68-67395. Benson, S. W. *Thermochemical Kinetics*; Wiley: New York, 1976.

(31) Gilbert, R. G.; Smith, S. C.; Jordan, M. J. T.; Unimol Program Suite, 1993.

(32) Gilbert, R. G.; Smith, S. C. *Theory of Unimolecular and Recombination Reactions*; Blackwell Scientific Publications: Oxford and Cambridge, UK, 1990.

(33) Li, Y.; Sun, J.; Han, K.; He, G.; Li, Z. *Chem. Phys. Lett.* **2006**, *232*, 421.

(34) Batt, L.; Robinson, G. N. *The Chemistry of Amino, Nitroso, and Nitro Compounds and their Derivatives*; Patai, S., Ed.; Wiley: New York, 1982.

(35) Wodtke, A. M.; Hintsa, E. J.; Lee, Y. T. *J. Phys. Chem.* **1986**, *90*, 3549.

JP806965P